Nuclear Medicine and Biology 43 (2016) 661–669

Contents lists available at ScienceDirect

Nuclear Medicine and Biology

journal homepage: www.elsevier.com/locate/nucmedbio

Comparison of biological properties of ^{99m}Tc-labeled cyclic RGD Peptide trimer and dimer useful as SPECT radiotracers for tumor imaging

Zuo-Quan Zhao [a], Yong Yang [a,b], Wei Fang [a,*], Shuang Liu [b,**]

[a] Department of Nuclear Medicine, Fuwai Hospital, the National Center for Cardiovascular Diseases, Chinese Academy of Medical Sciences and Peking Union Medical College, Beijing, China
[b] School of Health Sciences, Purdue University, West Lafayette, USA

ARTICLE INFO

Article history:
Received 25 January 2016
Received in revised form 12 February 2016
Accepted 22 February 2016

Keywords:
integrin $\alpha_v\beta_3$
^{99m}Tc-trimeric cyclic RGD peptide
tumor imaging
SPECT

ABSTRACT

Introduction: This study sought to evaluate a ^{99m}Tc-labeled trimeric cyclic RGD peptide (^{99m}Tc-4P-RGD$_3$) as the new radiotracer for tumor imaging. The objective was to compare its biological properties with those of ^{99m}Tc-3P-RGD$_2$ in the same animal model.
Methods: HYNIC-4P-RGD$_3$ was prepared by reacting 4P-RGD$_3$ with excess HYNIC-OSu in the presence of diisopropylethylamine. ^{99m}Tc-4P-RGD$_3$ was prepared using a kit formulation, and evaluated for its tumor-targeting capability and biodistribution properties in the BALB/c nude mice with U87MG human glioma xenografts. Planar and SPECT imaging studies were performed in athymic nude mice with U87MG glioma xenografts. For comparison purpose, ^{99m}Tc-3P-RGD$_2$ (a $\alpha_v\beta_3$-targeted radiotracer currently under clinical evaluation for tumor imaging in cancer patients) was also evaluated in the same animal models. Blocking experiments were used to demonstrate the $\alpha_v\beta_3$ specificity of ^{99m}Tc-4P-RGD$_3$.
Results: ^{99m}Tc-4P-RGD$_3$ was prepared with >95% RCP and high specific activity (~200 GBq/μmol). ^{99m}Tc-4P-RGD$_3$ and ^{99m}Tc-3P-RGD$_2$ shared almost identical tumor uptake and similar biodistribution properties. ^{99m}Tc-4P-RGD$_3$ had higher uptake than ^{99m}Tc-3P-RGD$_2$ in the intestines and kidneys; but it showed better metabolic stability. The U87MG tumors were clearly visualized by SPECT with excellent contrast with ^{99m}Tc-4P-RGD$_3$ and ^{99m}Tc-3P-RGD$_2$.
Conclusion: Increasing peptide multiplicity from 3P-RGD$_2$ to 4P-RGD$_3$ offers no advantages with respect to the tumor-targeting capability. ^{99m}Tc-4P-RGD$_3$ is as good a SPECT radiotracer as ^{99m}Tc-3P-RGD$_2$ for imaging $\alpha_v\beta_3$-positive tumors.

© 2016 Elsevier Inc. All rights reserved.

1. Introduction

Integrin $\alpha_v\beta_3$ is a receptor for the extracellular matrix proteins (e.g. collagen, fibrinogen, fibronectin, laminin and vitronectin) with one or more arginine-glycine-aspartic (RGD) tripeptide sequences. The $\alpha_v\beta_3$ is generally expressed at low levels on epithelial cells and mature endothelial cells, but it is overexpressed on the tumor cells and activated endothelial cells of neovasculature. Because of the role of $\alpha_v\beta_3$ in tumor angiogenesis and metastasis, cyclic RGD peptides are often used as $\alpha_v\beta_3$ antagonists for tumor therapy, and radiolabeled cyclic RGD peptides are utilized as "$\alpha_v\beta_3$–targeted" radiotracers for tumor imaging [1–10]. Over the last several years, we have been interested in radiolabeled multimeric cyclic RGD peptides as radiotracers for imaging $\alpha_v\beta_3$-positive tumors and related metastasis [11–29]. Multiple cyclic RGD moieties are utilized to maximize their $\alpha_v\beta_3$ binding affinity and tumor uptake of their corresponding radiotracers regardless of the attached isotope. We found that there are two important factors (bivalency and locally enhanced RGD concentration) contributing to the higher $\alpha_v\beta_3$ binding affinity of multimeric cyclic RGD peptides than their monomeric analogs [1,20,23]. The concentration factor exists

Abbreviations: HYNIC-OSu, sodium succinimidyl 6-(2-(2-sulfonatobenzaldehyde)hydrazono)nicotinate); ITLC, instant thin layer chromatography; MALDI, matrix-assisted laser desorption ionization; PET, positron emission tomography; RCP, radiochemical purity; SPECT, single photon emission computed tomography; RGD$_2$, E[c(RGDfK)]$_2$ = Glu[cyclo(Arg-Gly-Asp-D-Phe-Lys)]$_2$; RGD$_4$, E{E[c(RGDfK)]$_2$}$_2$ = Glu{E[cyclo(Arg-Gly-Asp-D-Phe-Lys)]$_2$}$_2$; 2P-RGD$_2$, E[PEG$_4$-c(RGDfK)]$_2$ = Glu[cyclo[Arg-Gly-Asp-D-Phe-Lys(PEG$_4$)]]$_2$ (PEG$_4$ = 15-amino-4,7,10,13-tetraoxapentadecanoic acid); 3P-RGD$_2$, PEG$_4$-E[PEG$_4$-c(RGKfD)]$_2$ = PEG$_4$-Glu[cyclo[Arg-Gly-Asp-D-Phe-Lys(PEG$_4$)]]$_2$; 4P-RGD$_3$, PEG$_4$-ACHDA[cyclo[Arg-Gly-Asp-D-Phe-Lys(PEG$_4$)]]$_3$ (ACHDA = 4-amino-4-(2-carboxyethyl)heptanedioic acid); HYNIC-4P-RGD$_3$, HYNIC-PEG$_4$-ACHDA[cyclo[Arg-Gly-Asp-D-Phe-Lys(PEG$_4$)]]$_3$ (HYNIC = 6-(2-(2-sulfonatobenzaldehyde)hydrazono)nicotinyl); ^{18}F-Alfatide-II, [^{18}F]AlF(NOTA-2P-RGD$_2$) (NOTA = 1,4,7-tritazacyclononane-1,4,7-triacetic acid); ^{99m}Tc-3P-RGD$_2$, [^{99m}Tc(HYNIC-3P-RGD$_2$)(tricine)(TPPTS)] (TPPTS = trisodium triphenylphosphine-3,3′,3″-trisulfonate); ^{99m}Tc-4P-RGD$_3$, [^{99m}Tc(HYNIC-4P-RGD$_3$)(tricine)(TPPTS)].

* Correspondence to: W. Fang, Department of Nuclear Medicine, Fuwai Hospital, the National Center for Cardiovascular Diseases, Chinese Academy of Medical Sciences and Peking Union Medical College, Beijing, China.
** Correspondence to: S. Liu, School of Health Sciences, Purdue University, 550 Stadium Mall Drive, West Lafayette, IN 47907. Tel.: +1 765 494 0236; fax: +1 765 496 1377.
E-mail addresses: nuclearfw@126.com (W. Fang), liu100@purdue.edu (S. Liu).

http://dx.doi.org/10.1016/j.nucmedbio.2016.02.006
0969-8051/© 2016 Elsevier Inc. All rights reserved.

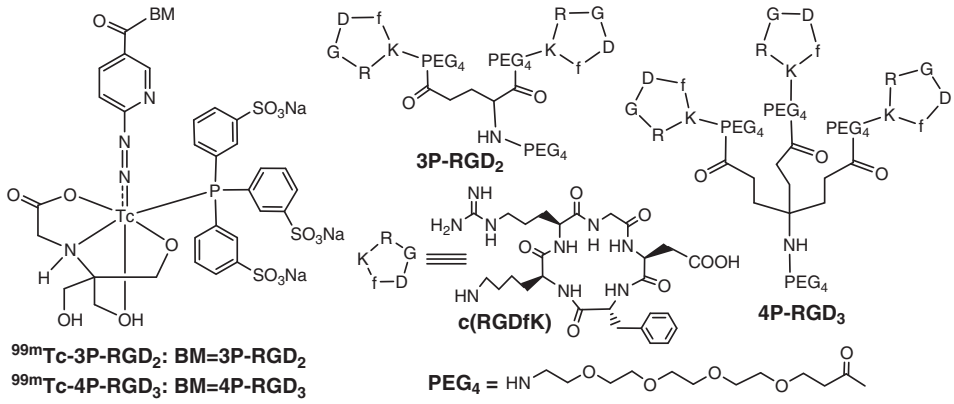

Fig. 1. Chemdraw structures of multimeric cyclic RGD peptides (3P-RGD_2 and 4P-RGD_3) and their ternary ligand complexes [^{99m}Tc(HYNIC-BM)(tricine)(TPPTS)] (BM = biomolecule; ^{99m}Tc-3P-RGD_2: BM = 3P-RGD_2; and ^{99m}Tc-4P-RGD_3: BM = 4P-RGD_3). ^{99m}Tc-4P-RGD_3 is the new SPECT radiotracer evaluated in this study. ^{99m}Tc-3P-RGD_2 is currently under intensive clinical evaluation for tumor imaging in cancer patients [31–35]. It was used for comparison purposes to study the impact of peptide multiplicity on tumor uptake and biodistribution properties in the same tumor-bearing animal model.

in all multimeric RGD peptides regardless of the linker length. The key to achieve bivalency is the distance between two cyclic RGD motifs. We also found that cyclic RGD tetramers (such as RGD_4) are actually bivalent in binding to the $\alpha_v\beta_3$ even though they have four identical cyclic c(RGDfK) motifs [20,23]. Among many of radiolabeled multimeric cyclic peptides, ^{99m}Tc-3P-RGD_2 (Fig. 1) and ^{18}F-Alfatide-II are currently under clinical evaluations as new radiotracers for tumor imaging in cancer patients [30–36]. Since ^{99m}Tc-3P-RGD_2 could be prepared in >95% radiochemical purity, it offers significant advantages over ^{18}F-Alfatide-II, which often requires post-labeling chromatographic purification [35,36]. ^{99m}Tc-3P-RGD_2 SPECT/CT has been used to quantify the tumor uptake [37–40], and to monitor the tumor growth [37,38], the progression of breast cancer lung metastases [39], and the pharmacological effects of antiangiogenic therapy [38,40].

In the literature, only a few radiolabeled cyclic RGD trimers were reported [41,42]. There was no comparison in biodistribution properties between the radiolabeled cyclic RGD dimers and trimers. With this in mind, we designed a new RGD peptide trimer (Fig. 1: 4P-RGD_3 = PEG_4-ACHDA[cyclo[Arg-Gly-Asp-D-Phe-Lys(PEG_4)]]$_3$; and ACHDA = 4-amino-4-(2-carboxyethyl)heptanedioic acid). ACHDA was used to bridge three c(RGDfK) moieties. Four PEG_4 linkers were used to enhance the hydrophilicity of ^{99m}Tc radiotracer and increase the distance between two neighboring c(RGDfK) moieties in 4P-RGD_3 so that it is able to achieve bivalency. In this report, we present the synthesis and biological evaluation of ^{99m}Tc-4P-RGD_3 (Fig. 1) as a new SPECT radiotracer for tumor imaging. ^{99m}Tc-4P-RGD_3 is the first ^{99m}Tc-labeled cyclic RGD peptide trimer. The main objective of this study was to compare the biodistribution and imaging properties of ^{99m}Tc-4P-RGD_3 and ^{99m}Tc-3P-RGD_2 in the same tumor-bearing animal model.

2. Experimental Section

2.1. Materials and Instruments

Tricine and trisodium triphenylphosphine-3,3′,3″-trisulfonate (TPPTS) were purchased from *Sigma/Aldrich* (St. Louis, MO), and were used without further purification. Cyclic RGD peptides RGD_2 (E[c(RGDfK)]$_2$ = Glu[cyclo(Arg-Gly-Asp-D-Phe-Lys)]$_2$) and 4P-RGD_3 (PEG_4-ACHDA{cyclo[Arg-Gly-Asp-D-Phe-Lys(PEG_4)]}$_3$) were custom-made by the Peptides International, Inc. (Louisville, KY). Sodium succinimidyl 6-(2-(2-sulfonatobenzaldehyde)hydrazono)nicotinate (HYNIC-OSu) was prepared according to literature method [43]. HYNIC-3P-RGD_2 and ^{99m}Tc-3P-RGD_2 were prepared using the procedure described in our previous report [14]. Na$^{99m}TcO_4$ was obtained from Cardinal HealthCare® (Indianapolis, IN). The MALDI (matrix-assisted laser desorption ionization) mass spectral data for HYNIC-4P-RGD_3 were collected on an Applied Biosystems Voyager DE PRO mass spectrometer (Framingham, MA), the Department of Chemistry, Purdue University.

2.2. HPLC Methods

HPLC Method 1 used a LabAlliance HPLC system (Scientific Systems, Inc., State College, PA) equipped with a UV/vis detector (λ = 254 nm) and Zorbax C_{18} column (9.4 mm × 250 mm, 100 Å pore size; Agilent Technologies, Santa Clara, CA). The flow rate was 2.5 mL/min with a mobile phase being 90% A and 10% B at 0 min to 80%A and 20% B at 5 min, and to 50%A and 50% B at 20 min. The radio-HPLC (Method 2) used an Agilent HP-1100 HPLC system (Agilent Technologies, Santa Clara, CA) equipped with a β-ram IN/US detector (Tampa, FL) and Zorbax C_8 column (4.6 mm × 250 mm, 300 Å pore size; Agilent Technologies, Santa Clara, CA). The flow rate was 1 mL/min. The mobile phase was isocratic for the first 5 min with 90% A (25 mM NH_4OAc, pH = 6.8) and 10% B (acetonitrile), followed by a gradient mobile phase going from 90% A and 10% B at 5 min to 40% A and 60% B at 20 min. The radiochemical purity was reported as the percentage of area for the peak at 15–16 min on each radio-HPLC chromatogram of ^{99m}Tc-3P-RGD_2 and ^{99m}Tc-4P-RGD_3. The instant thin layer chromatography (ITLC) used Gelman Sciences silica-gel strips and a 1:1 mixture of acetone and saline as the mobile phase. ^{99m}Tc-3P-RGD_2, ^{99m}Tc-4P-RGD_3 and $^{99m}TcO_4^-$ migrated to solvent front while [^{99m}Tc]colloid stayed at the origin. [^{99m}Tc]colloid was reported as the percentage of radioactivity at the origin over the total radioactivity on each strip.

2.3. HYNIC-4P-RGD_3

HYNIC-OSu (13.5 mg, 30 μmol) and 4P-RGD_3 (9.0 mg, 3 μmol) were dissolved in DMF (2 mL). After addition of excess DIEA (5 drops), the mixture was stirred at room temperature for 24 h. To the mixture was added 2 mL of water after completion of the reaction. The pH value was then adjusted to 3–4 using neat TFA. The product was separated from the reaction mixture by HPLC. Fractions at ~18 min were collected. Lyophilization of collected fractions afforded the expected product HYNIC-4P-RGD_3 as a white powder. The yield was 6.5 mg (~50%). MALDI-MS: m/z = 3295.8240 for $[M + H]^+$ (M = 3294.61 calcd. For $[C_{148}H_{227}N_{35}O_{48}S]$).

2.4. ^{99m}Tc-Labeling

To a lyophilized vial containing 20–25 μg HYNIC-RGD conjugate, 5 mg TPPTS, 6.5 mg tricine, 40 mg mannitol, 38.5 mg disodium succinate hexahydrate and 12.7 mg succinic acid was added 1.0–1.5 mL of

$Na^{99m}TcO_4$ solution (1110–1850 MBq in saline). The reconstituted vial was heated at 100 °C for 20 min. After cooling at room temperature for ~5 min, a sample of the resulting solution was analyzed by radio-HPLC (Method 2). The radiochemical purity (RCP) was always >95% for imaging and biodistribution studies. The solution stability was monitored by HPLC for 6 h.

2.5. Dose Preparation

For biodistribution, doses were prepared by dissolving ^{99m}Tc radiotracer in saline to a concentration of ~1 MBq/mL. For SPECT/CT imaging studies, doses were prepared by dissolving ^{99m}Tc radiotracer in saline to ~370 MBq/mL. In the blocking experiments, RGD_2 was dissolved in the dose solution to 3.5 mg/mL. The resulting dose solution was filtered with a 0.20 μm syringe-driven Millex-LG filter before being injected into animals. Each animal was injected with ~0.1 mL of the dose solution.

2.6. Cell Culture and Animal Models for Biodistribution

All animal experiments were performed in accordance with guidelines of Institutional Animal Care and Use Committee (IACUC) at Fu-Wai Hospital (Beijing, China). U87MG cell line was obtained from Peking Union Medical College. U87MG cells were cultured in DMEM (Dulbecco's modified eagle medium nonessential amino acids sodium pyruvate), supplemented with 10% fetal bovine serum (FBS) and 1% penicillin and streptomycin solution at 37 °C in a humidified atmosphere of 5% CO_2 in air, grown as monolayers, and were harvested or split when they reached 95% confluence to maintain exponential growth. Female BALB/c nude mice (4–5 weeks of age) were purchased from Department of Experimental Animals, Fu-Wai Hospital. The animal model was established by inoculating subcutaneously with 5×10^6 of U87MG cells into the shoulder flank of each animal. When the tumor volume reached ~400 mm^3 (~10 days after inoculation of U87MG cells), the tumor-bearing animals were used for biodistribution studies.

2.7. Biodistribution

Each tumor-bearing animal (16–20 g) was administered with ~0.1 MBq of ^{99m}Tc radiotracer (~2 ng HYNIC-3P-RGD_2 or HYNIC-4P-RGD_3) by tail vein injection. Five animals were sacrificed by sodium pentobarbital overdose (~200 mg/kg) at 5, 30, 60 and 120 min p.i. Blood was withdrawn from the heart. Tumors and normal organs (brain, eyes, heart, intestines, kidneys, liver, lungs, muscle and spleen) were harvested, washed with saline, dried with absorbent tissue, weighed, and counted on a Perkin Elmer Wizard – 1480 γ-counter (Shelton, CT). The organ uptake was calculated as the percentage of injected dose per gram of tissue (%ID/g). The blocking experiment was performed using RGD_2, a well-known integrin $\alpha_v\beta_3$ antagonist [1,3,7], as the blocking agent. Each animal was administered with ~0.1 MBq of ^{99m}Tc-4P-RGD_3 along with ~350 μg RGD_2 (~14 mg/kg). Biodistribution data (%ID/g) and tumor-to-background (T/B) ratios were expressed as the average plus standard deviation. Statistical analysis was performed by one-way analysis of variance (ANOVA) followed by the Newman–Keuls test for multiple comparisons. The level of significance was set at $p < 0.05$.

2.8. Cell Culture and Animal Model for Imaging Studies

Imaging studies were performed in compliance with the NIH animal experimentation guidelines (*Principles of Laboratory Animal Care*, NIH Publication No. 86–23, revised 1985). The protocol was approved by the Purdue University Animal Care and Use Committee (PACUC). U87MG, MDA-MB-435 and PC-3 cell lines were obtained from ATCC (Manassas, VA). U87MG cells were cultured in the Minimum Essential Medium, Eagle with Earle's Balanced Salt Solution (non-essential amino acids sodium pyruvate). PC-3 cells were cultured in the F-12 medium (GIBCO, Grand Island, NY). MDA-MB-435 cells were grown in the RPMI Medium 1640 with L-glutamine (GIBCO, Grand Island, NY). All tumor cell lines were supplemented with 10% fetal bovine serum and 1% penicillin and streptomycin solution, and grown at 37 °C in a humidified atmosphere of 5% CO_2 in air. Cells were grown as monolayers and were harvested or split when they reached 90% confluence. Female athymic *nu/nu* mice were purchased from Harlan at 4–5 weeks of age, and were implanted with 5×10^6 tumor cells in 0.1 mL of saline into the shoulder flanks of each animal for the U87MG and PC-3 models, or breast fat pads for the MDA-MB-435 model. When the tumor size was 0.1–0.5 g, and animals were used for imaging studies.

2.9. Planar Imaging

Each animal was administered with 300 ~ 500 μCi of ^{99m}Tc radiotracer in 0.1 mL saline via tail vein injection, anesthetized with intraperitoneal injection of ketamine (80 mg/kg) and xylazine (19 mg/kg), and then placed supine on a single head mini gamma camera (Diagnostic Services Inc., NJ) equipped with a parallel-hole, medium-energy and high-resolution collimator. The whole-body anterior images were acquired at 60 min p.i., and stored digitally in a 128 × 128 matrix. The acquisition count limits were set at 300 K. After completion of imaging, animals were sacrificed by sodium pentobarbital overdose (~200 mg/kg).

2.10. SPECT/CT Imaging

SPECT/CT images were obtained using a u-SPECT-II/CT scanner (Milabs, Utrecht, The Netherlands) equipped with a 1.0 mm multi-pinhole collimator. The tumor-bearing mouse was injected with ~37 MBq of ^{99m}Tc radiotracer (~ 1.0 μg HYNIC-conjugated cyclic RGD peptide) in 0.1 mL saline via the tail vein. At 60 min p.i., the animal was placed into a shielded chamber connected to an isoflurane anesthesia unit (Univentor, Zejtun, Malta). Anesthesia was induced using an air flow rate of 350 mL/min and ~3.0% isoflurane. After induction of anesthesia, the animal was immediately placed supine on the scanning bed. The air flow rate was then reduced to ~250 mL/min with ~2.0% isoflurane. Rectangular scan in the regions of interest (ROIs) from SPECT and CT were selected on the basis of orthogonal optical images provided by the integrated webcams. After SPECT acquisition (75 projections over 30 min per frame, 2 frames), the animal was then transferred into the attached CT scanner and imaged using the 'normal' acquisition settings (2 degree intervals) at 45 kV and 500 μA. After CT acquisition, the animal was allowed to recover in a lead-shielded cage.

2.11. Image Data Processing

SPECT reconstruction was performed using a POSEM (pixelated ordered subsets by expectation maximization) algorithm with 6 iterations and 16 subsets. CT data were reconstructed using a cone-beam filtered back-projection algorithm (NRecon v1.6.3, Skyscan). After reconstruction, the SPECT and CT data were automatically co-registered according to the movement of the robotic stage, and then re-sampled to equivalent voxel sizes. Co-registered images were further rendered and visualized using the PMOD software (PMOD Technologies, Zurich, Switzerland). A 3D-Guassian filter (0.8 mm FWHM) was applied to smooth noise, and the LUTs (look up tables) were adjusted for good visual contrast. The reconstructed images were visualized as both orthogonal slices and maximum intensity projections.

2.12. Radioactivity Quantification

Radiation sources of known amount of radioactivity were imaged and reconstructed using the same scanning protocol described above. A standard curve was generated to correlate the pixel intensities in the reconstructed images to the radioactivity as measured by a γ-counter. Tumor delineation was performed on CT and SPECT images according to the literature method

[37–40]. Briefly, the ROIs (regions of interest) were drawn manually to cover the entire tumor based on transverse view of the CT image. For the tumor delineation with SPECT, a threshold of 50% or more of the maximum pixel value on the SPECT image was chosen. In order to accurately represent the entire tumor, SPECT/CT was also employed to delineate the tumor ROIs. The tumor volume and radioactivity counts were generated by using the PMOD software (PMOD Technologies, Zurich, Switzerland). The amount of radioactivity in each tumor was calculated according to the above mentioned standard curve. The tumor uptake of ^{99m}Tc radiotracer was expressed the percentage of injected dose per gram (%ID/g, assuming the tumor density is ~1 g/cm^3), and was compared with the data from biodistribution in the same tumor-bearing animal model.

2.13. Metabolism

Athymic nude mice (n = 3) were used for metabolism study. Each animal was administered with ~10 MBq of ^{99m}Tc-4P-RGD$_3$ via the tail vein. The urine samples were collected at 30 min and 120 min p.i. by manual void, counted for total radioactivity, and were mixed with equal volume of 50% acetonitrile aqueous solution. The mixture was centrifuged at 8,000 rpm. The supernatant was collected, counted for the recovered radioactivity, and filtered with a 0.20 μm Millex-LG filter to remove foreign particles. The filtrate was analyzed by HPLC (Method 2). The feces samples were collected at 120 min p.i., counted for total radioactivity, and suspended in 20% acetonitrile aqueous solution. The mixture was vortexed for ~5 min. After centrifuging at 8,000 rpm, the supernatant was collected, counted for the recovered radioactivity, and filtered with a 0.20 μm syringe-driving Millex-LG filter unit to remove foreign particles. The filtrate was then analyzed by radio-HPLC (Method 2). The percentage of radioactivity recovery was >95% by γ-counting for both urine and feces samples.

2.14. Tissue Immunohistochemistry

Tumor tissues were harvested, immediately snap-frozen in OCT (optical cutting temperature) solution and cut into 5 μm-thick slices. After thorough drying at room temperature, the slides were fixed with ice-cold acetone for 10 min. The sections were then blocked and incubated with anti-integrin β_3 antibody (1:100, Santa Cruz) and CD31 antibody (1:100, BD Biosciences) for 1 h at room temperature. After washing, DyLight 594 and fluorescein isothiocyanate (FITC)-conjugated second antibodies (1:500, Jackson ImmunoResearch Inc., West Grove, PA) were added to link to integrin β_3 or CD31 primary antibody, respectively. The fluorescence was visualized with an Olympus BX51 fluorescence microscope (Olympus America Inc., Center Valley, PA). Phase contrast pictures were also obtained as the histological reference to illustrate the texture of the tumor or normal organ tissue and demonstrate the site of fluorescent staining. All the pictures were taken under 100× magnification. The same procedure was used to compare integrin β_3 expression levels in the U87MG tumor, kidneys, liver and lungs.

3. Results

3.1. Synthesis of HYNIC-4P-RGD$_3$

HYNIC-4P-RGD$_3$ was prepared from the reaction of 4P-RGD$_3$ with HYNIC-OSu in the presence of excess DIEA. The conjugation reaction was fast, and took ~24 h to complete at room temperature. HYNIC-4P-RGD$_3$ was purified by HPLC and characterized by ESI-MS. ESI-MS data was consistent with the proposed composition for HYNIC-4P-RGD$_3$. Its HPLC purity was >95% before being used for ^{99m}Tc-labeling.

3.2. Synthesis of ^{99m}Tc-4P-RGD$_3$

^{99m}Tc-4P-RGD$_3$ was prepared from the reaction of HYNIC-4P-RGD$_3$ with $^{99m}TcO_4^-$ in the presence of tricine and TPPTS coligands. ^{99m}Tc-labeling was accomplished by heating the reconstituted vial at 100 °C for 10–15 min. Fig. 2 shows radio-HPLC chromatograms of ^{99m}Tc-4P-RGD$_3$ in the kit matrix at 1 h and 6 h post-labeling. Its RCP was >95% without post-labeling purification. The specific activity was high (~200 GBq/μmol). ^{99m}Tc-4P-RGD$_3$ remained stable in the kit matrix for >6 h post-labeling.

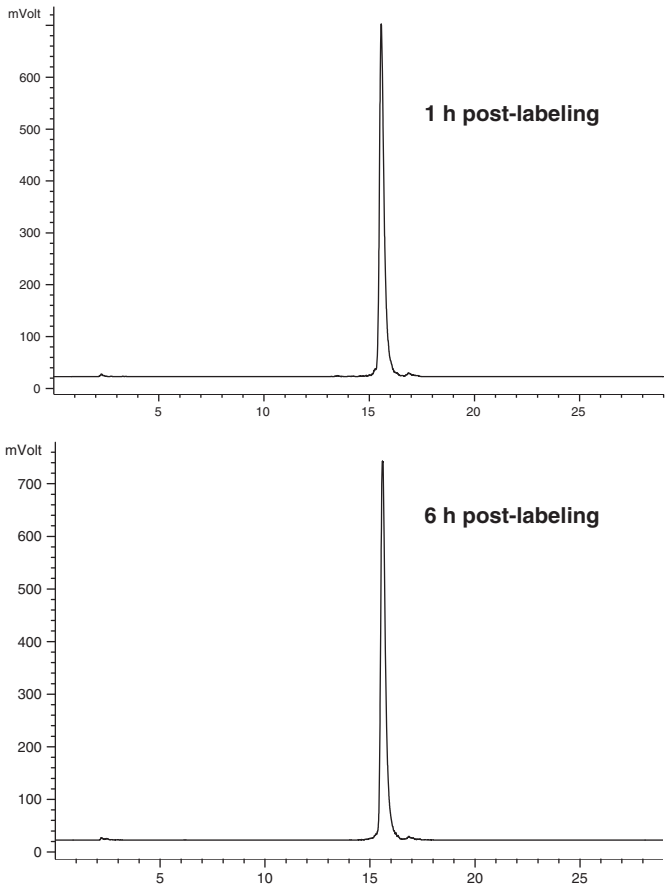

Fig. 2. Radio-HPLC chromatograms of ^{99m}Tc-4P-RGD$_3$ in the kit matrix at 1 h (top) and 6 h (bottom) post-labeling. The radiometric peak at ~15.6 min was from ^{99m}Tc-4P-RGD$_3$. Its radiochemical purity was always >95% without post-labeling chromatographic purification.

3.3. Biodistribution Properties

The selected biodistribution data for ^{99m}Tc-4P-RGD$_3$ are summarized in Table 1. ^{99m}Tc-3P-RGD$_2$ was evaluated in the same animal

Table 1
Selected biodistribution data and tumor-to-background ratios of ^{99m}Tc-4P-RGD$_3$ in BALB/c nude mice (n = 5) bearing U87MG human glioma xenografts. The tumor uptake (%ID/g) is reported as an average plus/minus the standard deviation.

Organ	5 min	30 min	60 min	120 min
Blood	4.43 ± 0.15	1.44 ± 0.18	0.88 ± 0.13	0.46 ± 0.04
Brain	0.51 ± 0.04	0.53 ± 0.23	0.28 ± 0.05	0.21 ± 0.03
Eyes	3.36 ± 0.22	3.20 ± 0.18	3.93 ± 0.78	2.77 ± 0.46
Heart	6.11 ± 0.31	4.07 ± 0.46	4.11 ± 0.31	2.51 ± 0.46
Intestine	19.06 ± 1.23	14.31 ± 1.43	15.93 ± 3.26	11.68 ± 1.22
Kidneys	55.62 ± 3.10	46.99 ± 4.18	45.81 ± 4.35	35.59 ± 8.55
Liver	9.89 ± 0.35	6.76 ± 1.03	6.11 ± 0.91	5.58 ± 0.97
Lungs	5.63 ± 3.66	4.93 ± 0.57	4.88 ± 0.43	2.64 ± 0.53
Muscle	3.05 ± 0.50	2.33 ± 0.37	3.28 ± 1.15	1.36 ± 0.16
Spleen	5.94 ± 0.55	6.15 ± 0.78	4.89 ± 1.10	5.13 ± 0.93
Tumor	5.42 ± 1.48	5.22 ± 0.17	5.17 ± 1.01	3.74 ± 0.51
Tumor/Blood	1.23 ± 0.34	3.69 ± 0.48	6.21 ± 2.34	8.21 ± 1.71
Tumor/Liver	0.55 ± 0.16	0.79 ± 0.11	0.87 ± 0.25	0.70 ± 0.19
Tumor/Lung	0.69 ± 0.15	1.07 ± 0.13	1.08 ± 0.25	1.45 ± 0.22
Tumor/Muscle	1.80 ± 0.48	2.29 ± 0.34	1.78 ± 0.69	2.79 ± 0.55

Table 2
Selected biodistribution data and tumor-to-background ratios of ^{99m}Tc-3P-RGD$_2$ in BALB/c nude mice (n = 5) bearing U87MG human glioma xenografts. The tumor uptake (%ID/g) is reported as an average plus/minus the standard deviation.

Organ	5 min	30 min	60 min	120 min
Blood	5.41 ± 0.53	1.54 ± 0.14	0.87 ± 0.10	0.32 ± 0.06
Brain	0.43 ± 0.08	0.41 ± 0.17	0.41 ± 0.05	0.23 ± 0.09
Eyes	2.74 ± 0.55	2.90 ± 22	2.57 ± 0.59	2.12 ± 0.86
Heart	6.39 ± 0.70	3.48 ± 0.45	3.13 ± 0.44	2.07 ± 0.75
Intestine	3.78 ± 0.52	4.24 ± 1.54	5.45 ± 1.47	3.37 ± 1.32
Kidneys	43.70 ± 3.27	32.89 ± 2.94	24.63 ± 3.59	19.05 ± 2.60
Liver	10.20 ± 1.12	5.82 ± 0.79	4.83 ± 0.60	4.52 ± 0.76
Lungs	8.64 ± 1.44	4.24 ± 0.87	3.50 ± 1.01	2.39 ± 0.71
Muscle	3.15 ± 0.64	2.25 ± 0.48	1.50 ± 0.49	1.23 ± 0.21
Spleen	5.84 ± 0.67	5.03 ± 0.45	4.02 ± 0.70	3.80 ± 0.50
Tumor	5.22 ± 0.72	6.77 ± 1.30	4.62 ± 0.57	3.93 ± 0.63
Tumor/Blood	0.96 ± 0.05	4.33 ± 0.12	5.86 ± 2.21	12.03 ± 3.62
Tumor/Liver	0.51 ± 0.03	1.16 ± 0.54	1.10 ± 0.54	0.84 ± 0.10
Tumor/Lung	0.61 ± 0.08	1.52 ± 0.74	1.33 ± 0.52	1.74 ± 0.63
Tumor/Muscle	1.68 ± 0.16	1.85 ± 1.38	2.25 ± 1.56	3.09 ± 0.40

model, and its selected biodistribution data are listed in Table 2. In general, ^{99m}Tc-4P-RGD$_3$ and ^{99m}Tc-3P-RGD$_2$ shared very similar biodistribution characteristics (Tables 1 and 2). The tumor uptake of ^{99m}Tc-4P-RGD$_3$ was almost identical to that of ^{99m}Tc-3P-RGD$_2$ over the 2 h study period (Fig. 3A). Increasing peptide multiplicity did not improve the radiotracer tumor uptake. In addition, they shared similar tumor/blood ratios (Fig. 3B). The most significant difference between ^{99m}Tc-4P-RGD$_3$ and ^{99m}Tc-3P-RGD$_2$ is their uptake values in intestines (Fig. 3C) and kidneys (Fig. 3D). It is important to note that the uptake of ^{99m}Tc-4P-RGD$_3$ and ^{99m}Tc-3P-RGD$_2$ in the U87MG glioma xenografted in BALB/c nude mice was significantly lower than that reported for ^{99m}Tc-3P-RGD$_2$ in previous studies [14,21,27]. To understand this difference, we performed immunohistochemical (IHC) staining on the tumor tissues obtained from U87MG-bearing BALB/c and athymic nude mice. We found that the U87MG tumor tissues obtained from the athymic nude mice had higher blood vessel density than that of the U87MG tissues from the BALB/c nude mice (Fig. 3E). Obviously,

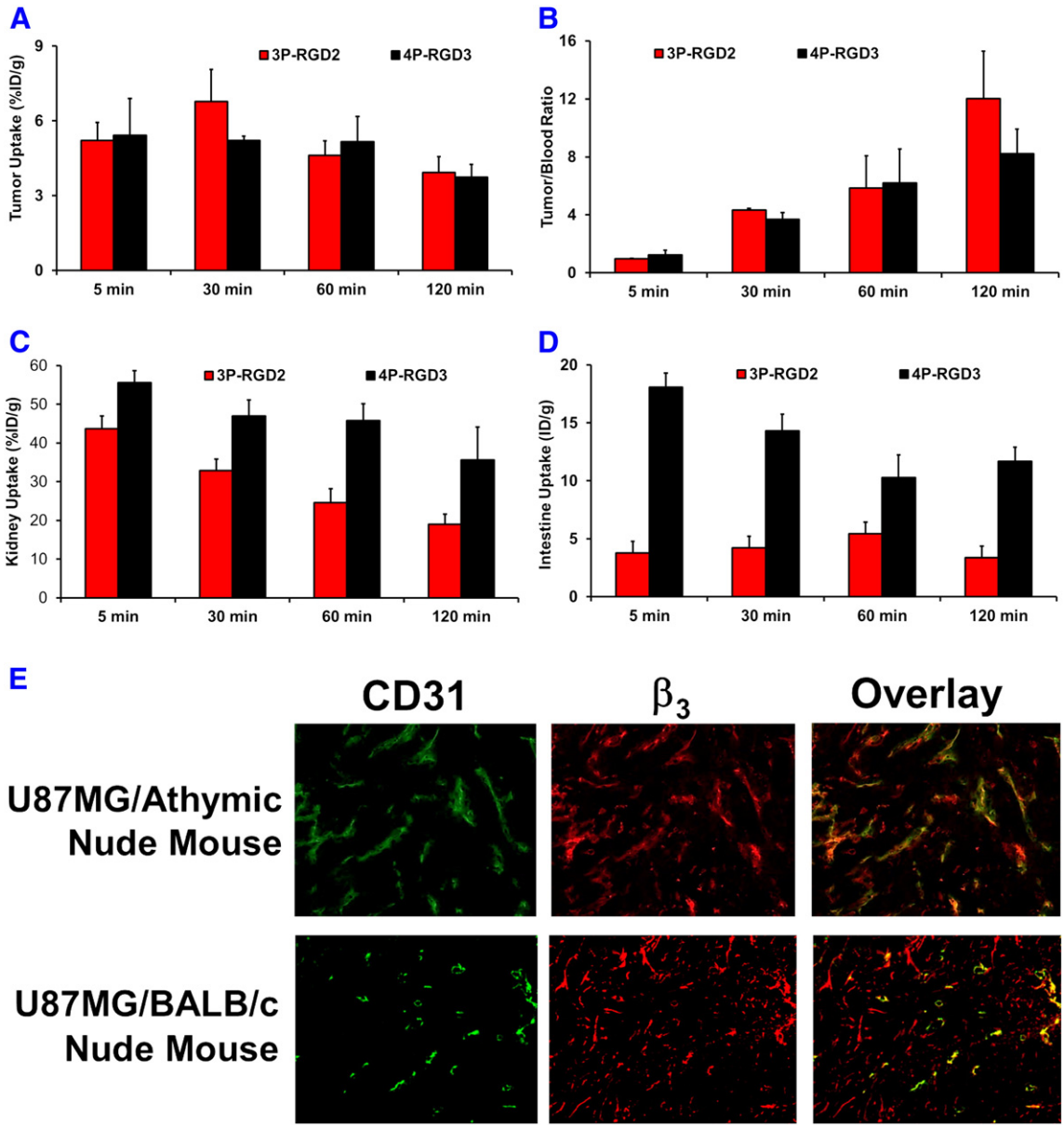

Fig. 3. Direct comparison of the uptake values of ^{99m}Tc-3P-RGD$_2$ and ^{99m}Tc-4P-RGD$_3$ in U87MG glioma tumors (**A**), kidneys (**C**) and intestine (**D**), along with their tumor/blood ratios (**B**) over the 2 h study period. The most significant difference between two radiotracers was their uptake in the intestine and kidneys. **E**: Representative microscopic fluorescence images of U87MG glioma tissues obtained from the athymic (high blood vessel density) and BALB/c (low blood vessel density) nude mice. In the overlay images, the green color indicates the presence of blood vessels, red color indicates the presence of β_3, and yellow color indicates the β_3 expressed on the tumor vasculature.

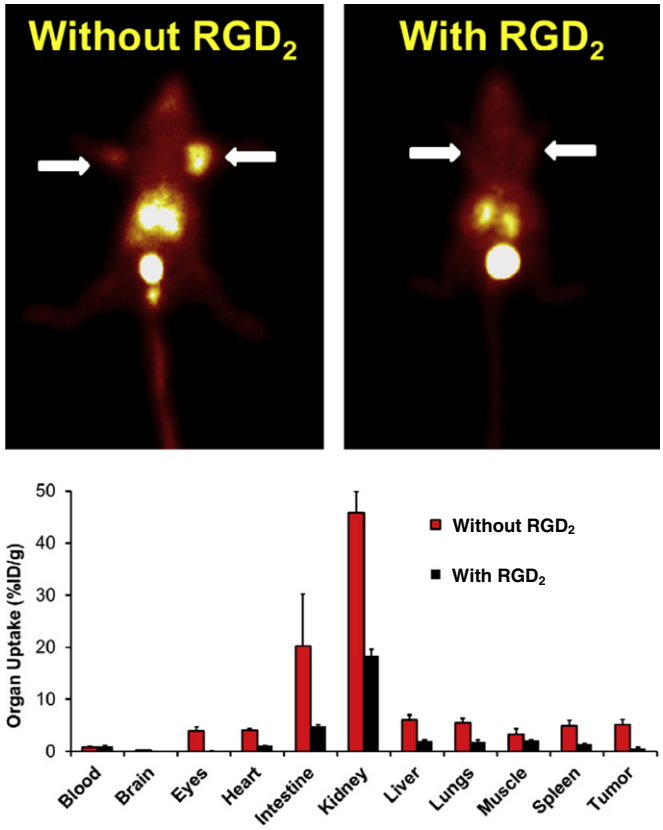

Fig. 4. Top: Planar images of the athymic nude mice bearing U87MG glioma xenografts administered with ^{99m}Tc-4P-RGD$_3$ with/without excess RGD$_2$ at 60 min post-injection. Arrows indicate the presence of tumors. **Bottom**: Direct comparison of the 60-min biodistribution data for ^{99m}Tc-4P-RGD$_3$ in BALB/c nude mice (n = 4) bearing U87MG glioma xenografts with/without excess RGD$_2$. Blocking experiments were designed to demonstrate the specificity of ^{99m}Tc-4P-RGD$_3$ for $\alpha_v\beta_3$.

the host animal species (e.g. BALB/c versus athymic nude mice) have significant impact on the radiotracer tumor uptake even if the same cancer cell line is used.

3.4. Integrin $\alpha_v\beta_3$ Specificity

Fig. 4**A** shows the 60-min planar images of U87MG-bearing athymic nude mice administered with ^{99m}Tc-4P-RGD$_3$ in the absence/presence of RGD$_2$ (350 μg/mouse). Co-injection of excess RGD$_2$ resulted in a significant reduction in the uptake of ^{99m}Tc-4P-RGD$_3$ in both U87MG glioma tumors and normal organs. Fig. 4**B** displays the selected 60-min biodistribution data of ^{99m}Tc-4P-RGD$_3$ in the absence/presence of RGD$_2$. Co-injection of excess RGD$_2$ (350 μg/mouse) blocked the tumor uptake of ^{99m}Tc-4P-RGD$_3$ (0.59 ± 0.28%ID/g with RGD$_2$ vs. 5.17 ± 1.01%ID/g without RGD$_2$). The normal organ uptake was also blocked by co-injection of excess RGD$_2$. Similar results were reported for ^{99m}Tc-3P-RGD$_2$ [14] and ^{111}In-labeled cyclic RGD dimers and tetramers [23].

3.5. SPECT/CT

SPECT/CT imaging studies were performed on ^{99m}Tc-4P-RGD$_3$ or ^{99m}Tc-3P-RGD$_2$ in athymic nude mice bearing U87MG glioma xenografts. ^{99m}Tc-3P-RGD$_2$ was used purely for comparison purposes. Fig. 5 displays the 3D and transverse views of SPECT/CT images of the U87MG-bearing nude mice administered with ~37 MBq of ^{99m}Tc-4P-RGD$_3$ or ^{99m}Tc-3P-RGD$_2$. The tumors were clearly visualized by SPECT/CT with excellent tumor-to-background contrast with both ^{99m}Tc-4P-RGD$_3$ and ^{99m}Tc-3P-RGD$_2$. These data clearly showed that ^{99m}Tc-4P-RGD$_3$ is as good as ^{99m}Tc-3P-RGD$_2$ for detection of the tumors. This conclusion is supported by the biodistribution data (Tables 1 and 2).

3.6. Monitoring $\alpha_v\beta_3$ Expression

Three animal models (U87MG, MDA-MB-435 and PC-3) were used to illustrate the ability of ^{99m}Tc-4P-RGD$_3$ to monitor $\alpha_v\beta_3$ expression. Fig. 6A compares transverse views of SPECT/CT images of the tumor-bearing mice administered with ^{99m}Tc-4P-RGD$_3$. The tumor uptake values follow the general ranking order of U87MG > MDA-MB-435 > > PC-3. Fig. 6B shows the overlay images of xenografted tumor tissues (U87MG, MDA-MB-435 and PC-3). The β_3 expression level (fluorescence density) was defined by the percentage of red-colored area over the total area. We found that the $\alpha_v\beta_3$ expression level followed the general trend: U87MG > MDA-MB-435 > > PC-3. Fig. 6C shows a plot of the %ID/g tumor uptake (radioactivity density) of ^{99m}Tc-4P-RGD$_3$ obtained from SPECT quantification and the $\alpha_v\beta_3$ expression levels (fluorescence density) in U87MG, MDA-MB-435 and PC-3 tumors, as determined from the quantification of fluorescent intensity. Apparently, there was a linear relationship between the %ID/g tumor uptake of ^{99m}Tc-4P-RGD$_3$ and the $\alpha_v\beta_3$ expression levels with R^2 being 0.98.

3.7. Metabolic Stability

Fig. 7 shows typical radio-HPLC chromatograms of ^{99m}Tc-4P-RGD$_3$ in saline before being injected into animal (A), in the urine at 30 min p.i. (B) and 120 min p.i. (C), and in the feces at 120 min p.i. (D). There were no metabolites detected in the urine sample over the 2 h study period for ^{99m}Tc-4P-RGD$_3$. More than 95% of ^{99m}Tc-4P-RGD$_3$ remained intact in the feces sample at 2 h p.i. The in vivo metabolic stability of ^{99m}Tc-4P-RGD$_3$ was better than that of ^{99m}Tc-3P-RGD$_2$, only 70% of which remained intact in the feces samples at 2 h p.i. [14].

4. Discussion

Previously, we found that cyclic RGD peptide dimers with the PEG$_4$ linkers (e.g. 3P-RGD$_2$) are bivalent in binding to the $\alpha_v\beta_3$ because of their better tumor-targeting capability than that of RGD$_2$, as indicated by their higher $\alpha_v\beta_3$-binding affinity and better tumor uptake of their radiotracers [13–29]. We also found that multimeric peptides are not necessarily multivalent in binding to the $\alpha_v\beta_3$, and multimerization of RGD peptides often leads to more radioactivity accumulation in the $\alpha_v\beta_3$-positive organs [20,23]. ^{99m}Tc-4P-RGD$_3$ represents the "missing link" between radiolabeled cyclic RGD peptide dimers and tetramers. In this study, we found that ^{99m}Tc-4P-RGD$_3$ and ^{99m}Tc-3P-RGD$_2$ shared almost identical tumor uptake (Fig. 3**A**) and similar biodistribution properties (Tables 1 and 2). Increasing peptide multiplicity from 3P-RGD$_2$ to 4P-RGD$_3$ offers no advantages in the tumor-targeting capability once bivalency is achieved. Similar conclusion was made with ^{111}In-labeled RGD tetramers [23]. The $\alpha_v\beta_3$ specificity of ^{99m}Tc-4P-RGD$_3$ has been demonstrated by blocking experiments (Fig. 4). ^{99m}Tc-4P-RGD$_3$ had higher uptake than ^{99m}Tc-3P-RGD$_2$ in the intestines (Fig. 3C) and kidneys (Fig. 3D). However, ^{99m}Tc-4P-RGD$_3$ has better metabolic stability (Fig. 7) than ^{99m}Tc-3P-RGD$_2$. The glioma tumors were clearly visualized by SPECT/CT with excellent contrast with both ^{99m}Tc-4P-RGD$_3$ and ^{99m}Tc-3P-RGD$_2$ (Fig. 6). Thus, ^{99m}Tc-4P-RGD$_3$ is as good a SPECT radiotracer as ^{99m}Tc-3P-RGD$_2$ for imaging $\alpha_v\beta_3$-positive tumors.

^{99m}Tc-4P-RGD$_3$ exhibited higher uptake in the intestines, liver and kidneys than the tumor (Table 1). However, these organs are not visualized in SPECT/CT image (Fig. 5). Similar results were reported for ^{99m}Tc-3P-RGD$_2$ in various tumor-bearing models [37–40]. We also found that the radioactivity accumulation in these organs could be different even in the same animal over a 35-day period [37]. One possible explanation for this discrepancy is that ^{99m}Tc-4P-RGD$_3$ has higher tumor uptake (8–12%ID/g) in the U87MG glioma xenografted in the athymic nude mice used for SPECT imaging. Alternatively, this discrepancy might be

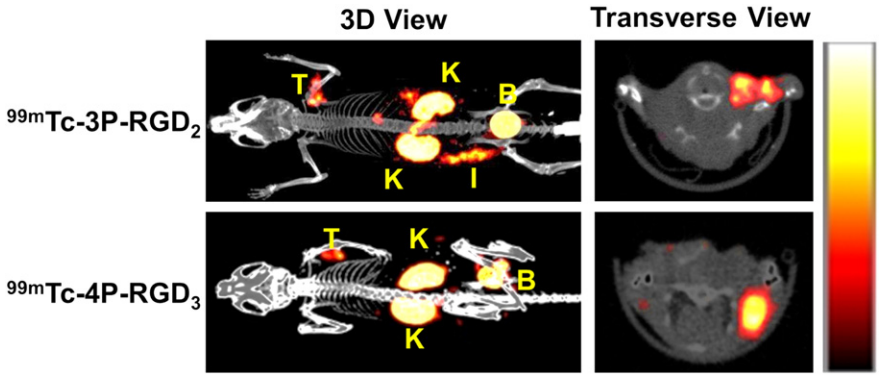

Fig. 5. The 3D and transverse views of SPECT/CT images of the athymic nude mice (B = bladder; I = intestine; K = kidney and T = tumor) bearing U87MG glioma xenografts. Each animal was administered with ~37 MBq of ^{99m}Tc radiotracer (~1.0 μg HYNIC-3P-RGD$_2$ or HYNIC-4P-RGD$_3$). All tumors were clearly visualized with excellent contrast using both radiotracers.

caused by different amounts of HYNIC-4P-RGD$_3$ co-injected with ^{99m}Tc-4P-RGD$_3$. For biodistribution, ~2 ng HYNIC-4P-RGD$_3$ was co-injected into each tumor-bearing mouse. For SPECT imaging, ~1 μg of HYNIC-4P-RGD$_3$ was co-administered with ^{99m}Tc-4P-RGD$_3$, and could cause partial blocking of ^{99m}Tc-4P-RGD$_3$ uptake in the organs (e.g. intestines, liver and kidneys) with limited total $\alpha_v\beta_3$ integrin population, as illustrated by β_3-staining of normal organ tissues [23]. The same explanation may also apply to ^{99m}Tc-3P-RGD$_2$.

It is well-established that the $\alpha_v\beta_3$ expression on both tumor cells and neovasculature contributes to the total tumor uptake of an $\alpha_v\beta_3$-targeted radiotracer regardless of the peptide multiplicity [20,23]. In our previous studies, we found that the percentage of contribution from the tumor neovasculature depends on the tumor type (e.g. U87MG vs. PC-3) [21,26]. The contribution from tumor neovasculature to the total tumor uptake of ^{99m}Tc-3P-RGD$_2$ is ~60% in the U87MG tumors xenografted in athymic nude mice [38]. In this study, we found

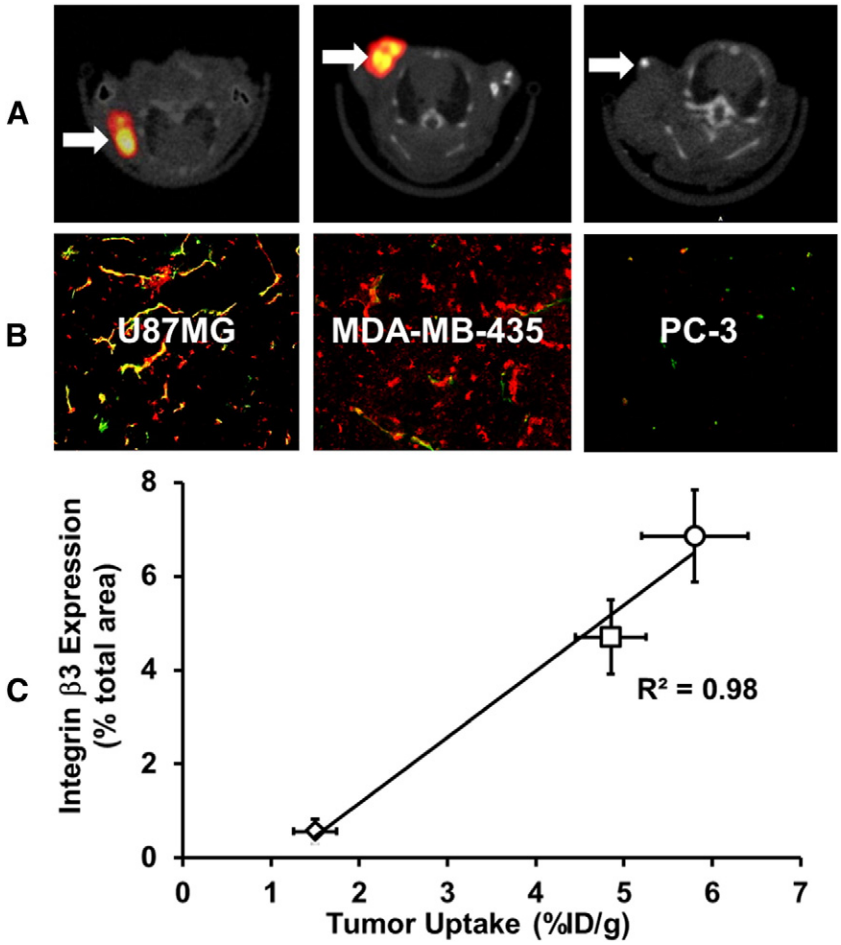

Fig. 6. A: Transverse views of SPECT/CT images from the tumor-bearing mice administered with ~50 MBq of ^{99m}Tc-4P-RGD$_3$. **B**: The overlay images of the xenografted U87MG, MDA-MB-435 and PC-3 tumor tissues. For β3 staining (red), frozen tissue slices were incubated with a β3 primary antibody followed by a DyLight 594-conjugated secondary antibody. For CD31 staining (green), slices were incubated with a CD31 primary antibody followed by a FITC-conjugated secondary antibody. In the overlay images, the green color indicates the presence of blood vessels, red color indicates the presence of β_3, and yellow color indicates the β_3 expressed on tumor neovasculature. **C**: Linear relationship between the tumor uptake of ^{99m}Tc-4P-RGD$_3$ from SPECT image semi-quantification and the relative β_3 expression levels (as represented by the % fluorescent intensity of red color over the total fluorescent intensity in the area) on three different tumor tissues to illustrate the capability of ^{99m}Tc-4P-RGD$_3$ to monitor the $\alpha_v\beta_3$ expression levels in tumor of different origin.

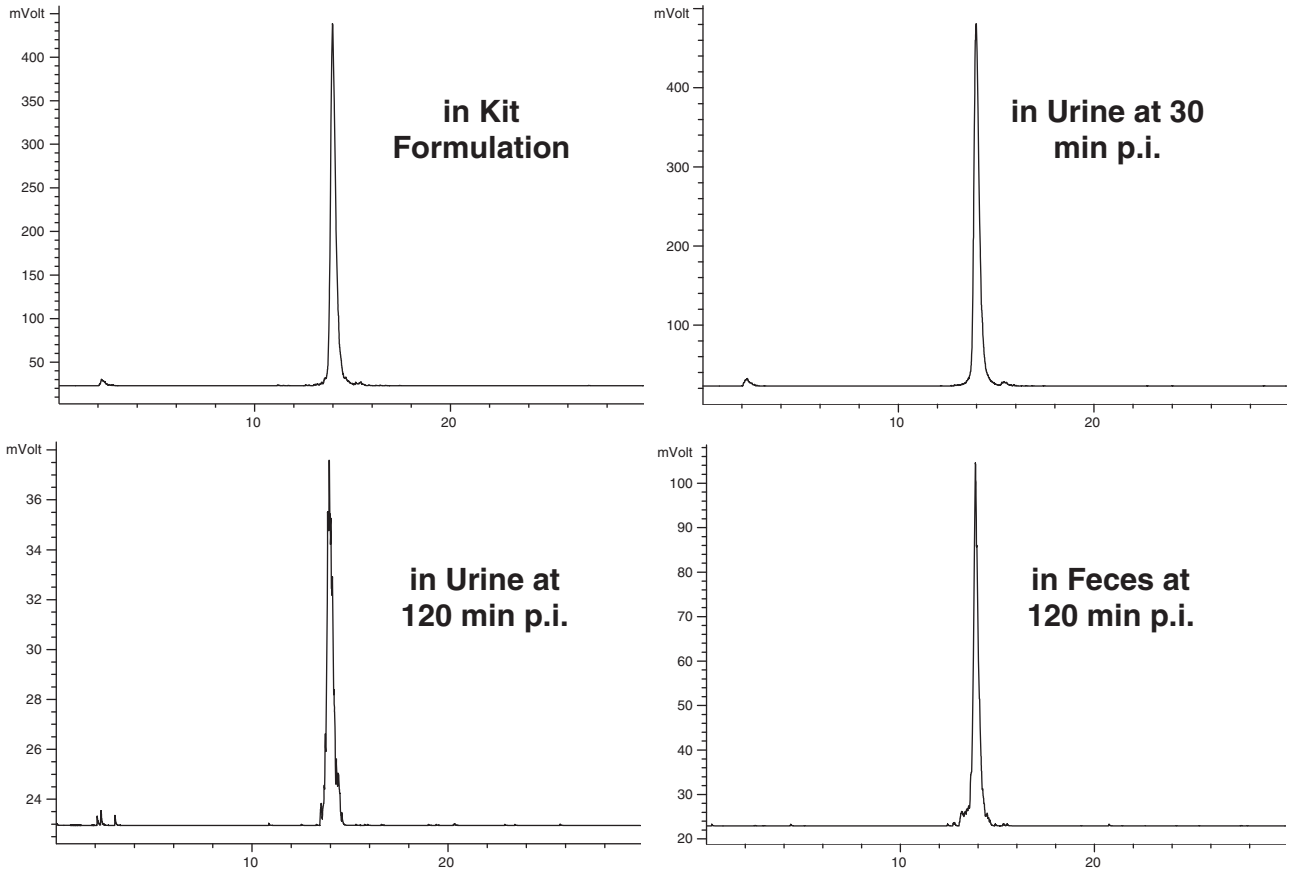

Fig. 7. Typical radio-HPLC chromatograms for ^{99m}Tc-4P-RGD$_3$ in the saline before injection, in the urine at 30 min p.i. and 120 min p.i., and in the feces at 120 min p.i.

that the tumors xenografted in the BALB/c nude mice had less uptake of ^{99m}Tc-3P-RGD$_2$ than those in the athymic nude mice. Since they share the same U87MG glioma cells, this difference is caused by the lower $\alpha_v\beta_3$ expression levels (Fig. 3) on the neovasculature of U87MG tumors xenografted in BALB/c nude mice, as determined by the IHC staining.

If the $\alpha_v\beta_3$–targeted radiotracer is used for accurate measurement of $\alpha_v\beta_3$ expression, there must be a linear relationship between the tumor uptake (radioactivity density) and $\alpha_v\beta_3$ levels (receptor density). The linear relationship between the %ID/g tumor uptake of ^{99m}Tc-4P-RGD$_3$ and $\alpha_v\beta_3$ expression levels (Fig. 6) clearly demonstrates its capability for noninvasive monitoring of the $\alpha_v\beta_3$ expression in tumor of different origin. In clinical settings, this capability is important for selection of the appropriate cancer patients who will benefit most from anti-$\alpha_v\beta_3$ and antiangiogenesis therapy. For example, if the cancer patient has high tumor uptake of ^{99m}Tc-4P-RGD$_3$, he/she would be likely responsive to the anti-$\alpha_v\beta_3$ treatment. Conversely, if the cancer patient shows little tumor uptake of ^{99m}Tc-4P-RGD$_3$, the therapy would not be effective regardless of the amount of anti-$\alpha_v\beta_3$ drug administered to the cancer patient.

5. Conclusion

In conclusion, ^{99m}Tc-4P-RGD$_3$ could be prepared in high radiochemical purity with specific activity. ^{99m}Tc-4P-RGD$_3$ and ^{99m}Tc-3P-RGD$_2$ shared almost identical tumor uptake and similar biodistribution properties. Even though ^{99m}Tc-4P-RGD$_3$ shows higher uptake in the intestines and kidneys, it has better metabolic stability than ^{99m}Tc-3P-RGD$_2$. ^{99m}Tc-4P-RGD$_3$ is as good a radiotracer as ^{99m}Tc-3P-RGD$_2$ for tumor imaging and noninvasive monitoring of the $\alpha_v\beta_3$ expression.

Conflict of interest

The authors confirm that there are no conflicts of interest associated with this publication.

Acknowledgement

This work was supported, in part, by Purdue University, R21 EB017237-01 (S.L.) from the National Institute of Biomedical Imaging and Bioengineering (NIBIB), and the grant number 81320108014 (W.F.) from National Natural Science Foundation of China.

References

[1] Liu S. Radiolabeled cyclic RGD peptide conjugates as radiotracers targeting multiple integrins. Bioconjug Chem 2015;26:1413–38.
[2] Beer AJ, Schwaiger M. Imaging of integrin $\alpha_v\beta_3$ expression. Cancer Metastasis Rev 2008;27:631–44.
[3] Liu S. Radiolabeled RGD peptides as integrin $\alpha_v\beta_3$-targeted radiotracers: maximizing binding affinity via bivalency. Bioconjug Chem 2009;20:2199–213.
[4] Stollman TH, Ruers TJM, Oyen WJG, Boerman OC. New targeted probes for radioimaging of angiogenesis. Methods 2009;48:188–92.
[5] Haubner R, Beer AJ, Wang H, Chen X. Positron emission tomography tracers for imaging angiogenesis. Eur J Nucl Med Mol Imaging 2010;37(Suppl. 1):S86–103.
[6] Dijkgraaf I, Boerman OC. Molecular imaging of angiogenesis with SPECT. Eur J Nucl Med Mol Imaging 2010;37(Suppl. 1):S104–13.
[7] Zhou Y, Chakraborty S, Liu S. Radiolabeled cyclic RGD peptides as radiotracers for imaging tumors and thrombosis by SPECT. Theranostics 2011;1:58–82.
[8] Beer AJ, Kessler H, Wester HJ, Schwaiger M. PET Imaging of integrin $\alpha_v\beta_3$ expression. Theranostics 2011;1:48–57.
[9] Danhier F, Le Breton A, Préat V. RGD-based strategies to target alpha(v)beta(3) integrin in cancer therapy and diagnosis. Mol Pharm 2012;9:2961–73.
[10] Tateishi U, Oka T, Inoue T. Radiolabeled RGD Peptides as integrin $\alpha_v\beta_3$–targeted PET tracers. Curr Med Chem 2012;19:3301–9.

[11] Dijkgraaf I, Liu S, Kruijtzer JA, Soede AC, Oyen WJG, Liskamp RM, et al. Effect of linker variation on the in vitro and in vivo characteristics of an ^{111}In-labeled RGD Peptide. Nucl Med Biol 2007;34:29–35.
[12] Dijkgraaf I, Kruijtzer JA, Liu S, Soede AC, Oyen WJG, Corstens FH, et al. Improved targeting of the $\alpha_v\beta_3$ integrin by multimerization of RGD peptides. Eur J Nucl Med Mol Imaging 2007;34:267–73.
[13] Shi J, Wang L, Kim YS, Zhai S, Liu Z, Chen X, et al. Improving tumor uptake and excretion kinetics of ^{99m}Tc-labeled cyclic arginine-glycine-aspartic (RGD) dimers with triglycine linkers. J Med Chem 2008;51:7980–90.
[14] Wang L, Shi J, Kim YS, Zhai S, Jia B, Zhao H, et al. Improving tumor targeting capability and pharmacokinetics of ^{99m}Tc-labeled cyclic RGD dimers with PEG_4 linkers. Mol Pharm 2009;6:231–45.
[15] Shi J, Wang L, Kim YS, Zhai S, Jia B, Wang F, et al. ^{99m}TcO(MAG_2-$3G_3$-dimer): A new integrin $\alpha_v\beta_3$-targeted radiotracer with high tumor uptake and favorable pharmacokinetics. Eur J Nucl Med Mol Imaging 2009;36:1874–84.
[16] Shi J, Kim YS, Zhai S, Liu Z, Chen X, Liu S. improving tumor uptake and pharmacokinetics of ^{64}Cu-labeled cyclic RGD dimers with triglycine and PEG_4 linkers. Bioconjug Chem 2009;20:750–9.
[17] Shi J, Kim YS, Chakraborty S, Jia B, Wang F, Liu S. 2-mercaptoacetylglycylglycyl (MAG_2) as a bifunctional chelator for ^{99m}Tc-labeling of cyclic RGD dimers: effects of technetium chelate on tumor uptake and pharmacokinetics. Bioconjug Chem 2009;20:1559–68.
[18] Liu Z, Niu G, Shi J, Liu S, Wang F, Chen X. ^{68}Ga-labeled cyclic RGD dimers with Gly_3 and PEG_4 linkers: promising agents for tumor integrin $\alpha_v\beta_3$ PET imaging. Eur J Nucl Med Mol Imaging 2009;36:947–57.
[19] Liu Z, Liu S, Wang F, Chen X. Noninvasive imaging of tumor integrin expression using ^{18}F-labeled RGD dimer peptide with PEG_4 linkers. Eur J Nucl Med Mol Imaging 2009; 36:1296–307.
[20] Chakraborty S, Liu S, Kim YS, Shi J, Zhou Y, Wang F. Evaluation of ^{111}In-labeled cyclic RGD peptides: tetrameric not tetravalent. Bioconjug Chem 2011;21:969–78.
[21] Zhou Y, Kim YS, Chakraborty S, Shi J, Gao H, Liu S. ^{99m}Tc-labeled cyclic RGD peptides for noninvasive monitoring of tumor integrin $\alpha_v\beta_3$ expression. Mol Imaging 2011; 10:386–97.
[22] Shi J, Jia B, Kim YS, Chakraborty S, Zhou Y, Wang F, et al. Impact of bifunctional chelators on biological properties of ^{111}In-labeled cyclic peptide RGD dimers. Amino Acids 2011;41:1059–70.
[23] Shi J, Zhou Y, Chakraborty S, Kim YS, Jia B, Wang F, et al. Evaluation of ^{111}In-labeled cyclic RGD peptides: effects of peptide and PEG_4 multiplicity on their tumor uptake, excretion kinetics and metabolic stability. Theranostics 2011;1:322–40.
[24] Jacobson O, Zhu L, Niu G, Szajek L, Ma Y, Sun X, et al. MicroPET imaging of integrin $\alpha_v\beta_3$ expressing tumors using ^{89}Zr-RGD peptides. Mol Imaging Biol 2011;13: 1224–33.
[25] Zhou Y, Kim YS, Lu X, Liu S. Evaluation of ^{99m}Tc-labeled cyclic RGD dimers: impact of cyclic RGD peptides and ^{99m}Tc chelates on biological properties. Bioconjug Chem 2012;23:586–95.
[26] Ji S, Zhou Y, Shao G, Liu S. $(HYNIC)_2$K: A bifunctional chelator useful for ^{99m}Tc-labeling of small biomolecules. Bioconjug Chem 2013;24:701–11.
[27] Ji S, Czerwinski A, Zhou Y, Shao G, Valenzuela F, Sowiński P, et al. ^{99m}Tc-galacto-RGD_2: a ^{99m}Tc-labeled cyclic RGD peptide dimer useful for tumor imaging. Mol Pharm 2013;10:3304–14.
[28] Yang Y, Ji S, Liu S. Impact of multiple negative charges on blood clearance and biodistribution characteristics of ^{99m}Tc-labeled dimeric cyclic RGD peptides. Bioconjug Chem 2014;25:1720–9.
[29] Zheng Y, Ji S, Yang Y, Tomaselli E, Liu S. ^{111}In-labeled cyclic RGD peptides useful as integrin $\alpha_v\beta_3$-targeted radiotracers for breast tumor imaging. Nucl Med Biol 2015; 42:137–45.
[30] Ma Q, Ji B, Jia B, Gao S, Ji T, Wang X, et al. Differential diagnosis of solitary pulmonary nodules using ^{99m}Tc-3P-RGD scintigraphy. Eur J Nucl Med Mol Imaging 2011;38: 2145–52.
[31] Zhu Z, Miao W, Li Q, Dai H, Ma Q, Wang F, et al. ^{99m}Tc-3PRGD2 for integrin receptor imaging of lung cancer: a multicenter study. J Nucl Med 2012;53:716–22.
[32] Zhao D, Jin X, Li F, Liang J, Lin Y. Integrin $\alpha_v\beta_3$ imaging of radioactive iodine–refractory thyroid cancer using ^{99m}Tc-3PRGD2. J Nucl Med 2012;53:1872–7.
[33] Ma Q, Chen B, Gao S, Ji T, Wen Q, Song Y, et al. ^{99m}Tc-3P4-RGD2 scintimammography in the assessment of breast lesions: comparative study with ^{99m}Tc-MIBI. PLoS One 2014;9:e108349.
[34] Liu L, Song Y, Gao S, Ji T, Zhang H, Ji B, et al. ^{99m}Tc-3PRGD2 scintimammography in palpable and nonpalpable breast lesions. Mol Imaging 2014;13:1–7.
[35] Guo J, Guo N, Lang L, Kiesewetter DO, Xie Q, Li Q, et al. ^{18}F-alfatide II and ^{18}F-FDG dual-tracer dynamic PET for parametric, early prediction of tumor response to therapy. J Nucl Med 2014;55:154–60.
[36] Yu C, Pan D, Mi B, Xu Y, Lang L, Niu G, et al. ^{18}F- Alfatide II PET/CT in healthy humans and patients with brain metastases. Eur J Nucl Med Mol Imaging 2015;42:2021–8.
[37] Shao G, Zhou Y, Liu S. Monitoring glioma growth and tumor necrosis with u-SPECT-II/CT for by targeting integrin $\alpha_v\beta_3$. Mol Imaging 2013;12:39–48.
[38] Ji S, Zhou Y, Shao G, Liu S, Voorbach MJ, Luo Y, et al. Monitoring tumor response to linifanib therapy with SPECT/CT using the $\alpha_v\beta_3$-targeted radiotracer ^{99m}Tc-3P-RGD_2. J Pharmacol Exp Ther 2013;346:251–8.
[39] Zhou Y, Shao G, Wang F, Liu S. Imaging breast cancer lung metastasis by u-SPECT-II/CT with an integrin $\alpha_v\beta_3$-targeted radiotracer ^{99m}Tc-3P-RGD_2. Theranostics 2012;2: 577–87.
[40] Ji S, Zheng Y, Shao G, Zhou Y, Liu S. Integrin $\alpha_v\beta_3$–targeted radiotracer ^{99m}Tc-3P-RGD_2 useful for noninvasive monitoring of breast tumor response to antiangiogenic linifanib therapy but not anti-integrin $\alpha_v\beta_3$ RGD_2 therapy. Theranostics 2013;3:816–30.
[41] Knetsch PA, Zhai C, Rangger C, Blatzer M, Haas H, Kaeopookum P, et al. [^{68}Ga]FSC-$(RGD)_3$ A trimeric RGD peptide for imaging $\alpha_v\beta_3$ integrin expression based on a novel siderophore derived chelating scaffold-synthesis and evaluation. Nucl Med Biol 2015;42:115–22.
[42] Kubasa H, Schäfera M, Bauder-Wüsta U, Edera M, Oltmannsa D, Haberkornb U, et al. Multivalent cyclic RGD ligands: influence of linker lengths on receptor binding. Nucl Med Biol 2010;37:885–91.
[43] Harris TD, Sworin M, Williams N, Rajopadhye M, Damphousse PR, Glowacka D, et al. Synthesis of stable hydrazones of a hydrazinonicotinyl-modified peptide for the preparation of ^{99m}Tc-labeled radiopharmaceuticals. Bioconjug Chem 1998;10:808–14.